



### **Science Arts & Métiers (SAM)**

is an open access repository that collects the work of Arts et Métiers Institute of Technology researchers and makes it freely available over the web where possible.

This is an author-deposited version published in: <https://sam.ensam.eu>  
Handle ID: <http://hdl.handle.net/10985/6815>

#### **To cite this version :**

Benoit COSSON, Luc CHEVALIER, Gilles REGNIER - Simulation of the stretch blow moulding process: from the modelling of the microstructure evolution to the end-use elastic properties of polyethylene terephthalate bottles - International Journal of Material Forming - Vol. 39-53, n°1, p.5 - 2012

Any correspondence concerning this service should be sent to the repository

Administrator : [scienceouverte@ensam.eu](mailto:scienceouverte@ensam.eu)



# Simulation of the stretch blow moulding process: from the modelling of the microstructure evolution to the end-use elastic properties of polyethylene terephthalate bottles

Benoit Cosson · Luc Chevalier · Gilles Régnier

**Abstract** The whole stretch blow-moulding process of PET bottles is simulated at the usual process temperature in order to predict the elastic end-use properties of the bottles. An anisotropic viscoplastic constitutive law, coupled with microscopic variables, is identified from uniaxial tensile tests performed at different strain rates and temperatures. The microstructure evolution is characterised by crystallinity measurements from interrupted tests and frozen samples. For each specimen tested, the Young modulus is measured at room temperature. Numerical simulations of the blow moulding process are run using the C-NEM method. A micromechanical modelling is post-processed after the simulation to predict the elastic properties. Predictions of Young modulus distributions in bottles are in agreement with the ones measured on blow-moulded bottles.

**Keywords** Stretch blow-moulding process · Polyethylene terephthalate · Induced microstructure · Process simulation · Elastic properties

## Introduction

Polyethylene terephthalate (PET) is a thermoplastic (saturated polyester) that can be found either in an amorphous or a semi-crystalline state. Its microstructure exhibits therefore a mix of an amorphous phase and a crystalline one, with a given ratio, ranging from nearly zero to about 45 % (fully crystallized PET). Since, Daubeny et al. [1] who first published on PET properties, many authors have studied morphology changes of the PET. Without deformation, thermal or quiescent crystallisation occurring for temperatures between  $T_g$  and  $T_m$ , leads to a spherulitic microstructure like all semi-crystalline polymers. Benatmane [2] showed that the spherulites size depends on the cooling rate or the crystallisation temperature. The size of the spherulites ranges from  $10^{-6}$  to  $10^{-4}$  m which is enough to opacify the material. One can imagine that the kinetics of thermal crystallization for isotropic amorphous PET is very slow for the blow moulding temperature range (Hieber [3]). Asano and Seto [4] presented a study on drawn PET where it is shown that kinetics are very sensitive to chains orientation. Fisher and Fakirov [5] confirmed these results by WAXS measurements: quiescent crystallization could not be totally neglected during stretch blow moulding.

Strain also induces crystallization of PET during shear or tension loadings. From uniaxially stretched PET, Shen et al. [6] showed that alignment of macromolecules induces a change from cis- to trans-conformation. Spiby et al. [7] made infra-red measurements that confirmed this result on PET and other polymeric materials. This change of conformation induces a partial crystallization: benzene rings tend to align in a plane parallel to the principal directions of the mechanical solicitation (Lapersonne et al. [8]). The chains are organized at first in micellar structures

---

B. Cosson · L. Chevalier (✉)  
Laboratoire Modelisation Simulation Multi Echelle  
(MSME, UMR 8208 CNRS), Université Paris-Est,  
5 bd Descartes, Champs sur Marne,  
77454 Marne-la-Vallée, France  
e-mail: luc.chevalier@univ-paris-est.fr

G. Régnier  
Arts et Métiers ParisTech,  
Laboratoire des Procédés et Ingénierie en Mécanique  
et Matériaux (PIMM, UMR CNRS 8006),  
151 bd de l'Hôpital,  
75013 Paris, France

and then in crystalline lamellae. The limited dimensions of these structures (0.1–0.9 nm) keep the good transparency of the stretched and crystallized PET.

This strain induced crystallization has been observed for various strain states: Pople et al. [9] have studied induced crystallization and microstructure evolution during simple shear thanks to synchrotron X-ray measurements; Titomanlio et al. [10] has modelled this phenomenon in injection moulding simulations. Salem [11] has studied the influence of the strain rate on induced crystallization during hot drawing of PET film. Marco et al. [12] studied plane tension, equibiaxial or sequenced biaxial tension tests at constant speed. Le Bourvellec and Beautemps [13] managed to draw PET at constant load while Vigny et al. [14] provided results for plane tension tests at constant strain rate. Molecular mechanisms appear to be identical in all these studies but the induced microstructure highlights differences on crystallinity ratio, amorphous and crystalline chains orientation and crystals size. In a more recent study, Hanley et al. [15] collected SAXS data with a 100  $\mu\text{m}$  square X-ray beam in the petaloid bases of PET bottles and established a molecular morphology function of the position across the base and the topology. An amorphous region was identified in the base centre (i.e., close to the injection point of the preform) close to the biaxially orientated, and crystalline regions of the feet and valleys of the bottle bases. For bottles that had split under load, the transition between these two regions displayed uniaxial molecular orientation that would lead to reduced mechanical strength in the circumferential direction. More recently, Picard and Billon [16] followed, by WAXS and SAXS, the microstructure evolution of blown parts and clearly showed that the microstructure can differ along the bottle and from one processing condition to another. Differences can be observed on crystalline orientation, periodic arrangement at the level of lamellae and long period. Despite the high level of strain and evidence of strain hardening occurring during blowing, no perfect crystalline pattern has been observed, excepted in very thick zones. Interrupted tensile tests followed by sample quenching, demonstrates that strain hardening is not correlated to perfect crystallisation. Picard and Billon [16] suggested that this strain hardening effect was related to the evolution of a mesophase exhibiting a higher density than the amorphous phase.

Consequently, the final mechanical properties of stretch blow-moulded PET bottles are largely dependent on the history of deformation process, as shown in Chevalier et al. [17]. The knowledge of these properties is necessary to assess the ability of bottles to resist to internal pressure or palletizing. To design a bottle, under constraint of minimizing weight, the try-tests procedure starting from the design of the preform is very long and expensive. Another alternative procedure to design a bottle is to use numerical

simulations and numerous authors have proposed simulations of the injection stretch blow moulding process (see for example Mir et al. [18], Pham et al. [19], Haddad et al. [20], Bagherzadeh et al. [21], Michaeli and Leopold [22] or Menary et al. [23]) Since the behaviour exhibits a strong strain hardening effect, Marckma et al. [24] for example proposed to use a hyperelastic modelling. This is not satisfactory because it fails to represent the speed influence. Gorlier et al. [25] did take into account the speed effect by introducing elastics characteristics depending on the strain rate which makes little sense in terms of microscopic mechanism. On the other hand, Schmidt et al. [26] for example, ran stretch blow moulding simulations using a viscoelastic constitutive law. Even if the Maxwell like model was extended to a high level of strain by the use of an Oldroyd time derivation, the behaviour does not model the strain hardening effect and cannot reproduce the shape evolution of the preform. Considering the monotonous evolution of the strain during the blowing process and the quick cooling of the material when coming in contact with the mould, Chevalier and Marco [27] proposed a simple viscoplastic modelling identified on uniaxial and biaxial tension tests to simulate free inflation of the preform. This modelling has been used by Bordival et al. [28] in a numerical procedure based on simulations of the heating phase and the blowing phase performed to optimise the stretch blow moulding process. This simple model of the PET behaviour that generalizes the G'Sell-Jonas constitutive law in 3D, takes into account the strain-hardening effect and the influence of the strain rate. Recently, Cosson et al. [29], proposed an anisotropic version of this viscoplastic modelling.

Buckley and Jones [30] present a non linear visco-elastic model used in [23] for example to simulate the injection stretch blow moulding process. Mir et al. [18] for example, proposed an elasto-viscoplastic modelling which enables the determination of the internal stresses after blowing. A review of visco-elastic modelling of highly elastic flows of amorphous thermoplastics proposed by Figiel and Buckley [31] shows the way to improve such a modelling. Nevertheless, none of these models is coupled to microstructural changes: molecular orientation and crystallinity.

Microstructure evolution and induced properties are strongly coupled. Consequently, only a modelling that takes into account the evolution of the microstructure in the model and also the influence of the strain variations on the microstructure allows the prediction of end-use properties. In this study we propose a full stretch blow moulding simulation package which is able to model the crystalline microstructure evolution and predict the elastic behaviour of the final bottle.

In “**Experimental**”, the experiment is described: the material, the uniaxial tensile tests which aim to identify

the constitutive law of material during the process, the free-blowing of PET preforms and the measurements of final elastic properties. In “Material behaviour modelling”, the modelling of the material behaviour is presented. The constitutive law of PET during blowing and its coupling with the evolution of the crystalline microstructure is established. Then, considering the predicted induced crystalline microstructure, a micromechanical prediction of the elastic properties of stretched-blown PET at ambient temperature is determined is post-processed. In “Simulations”, the complete simulation process is described and the predicted elastic properties are compared to measurements.

## Experimental

### Material and sample preparation

The polymer used for this study is a PET Arnite D00301 (Intrinsic viscosity=70 dl/g) provided by DSM. Tensile samples are parallelepipedic bars with an initial cross section of 4 mm by 10 mm and a useful length of 30 mm. Specimen and preforms (Fig. 1) have been injection moulded following recommendation of DMS: the mould was regulated at 15°C to obtain quasi-amorphous tensile samples and preforms. The injection temperature was 290°C and a holding pressure of 40 MPa was maintained during 10 s. Injected preforms have been injection moulded by Sidel group.

The surfaces of tensile specimens were machined to remove the oriented skin layer in order to obtain a homogeneous sample and a quicker sample heating. The final thickness of the sample was 1 mm. After this preparation, specimens are nearly amorphous and the crystallinity, measured by densitometry, is lower than 2% throughout.

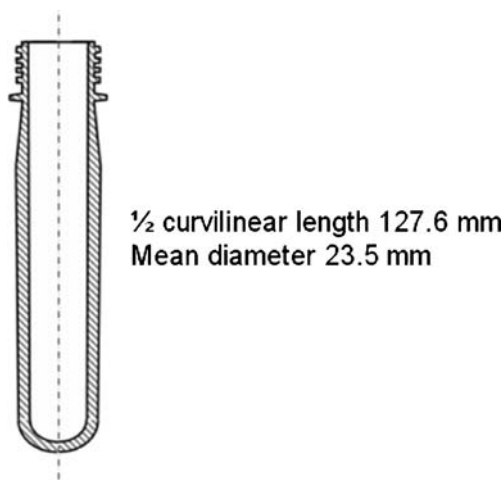


Fig. 1 Geometry of the studied injected preforms (2 L)

### Tensile tests

#### *Uniaxial tensile tests to identify the PET behaviour during blowing*

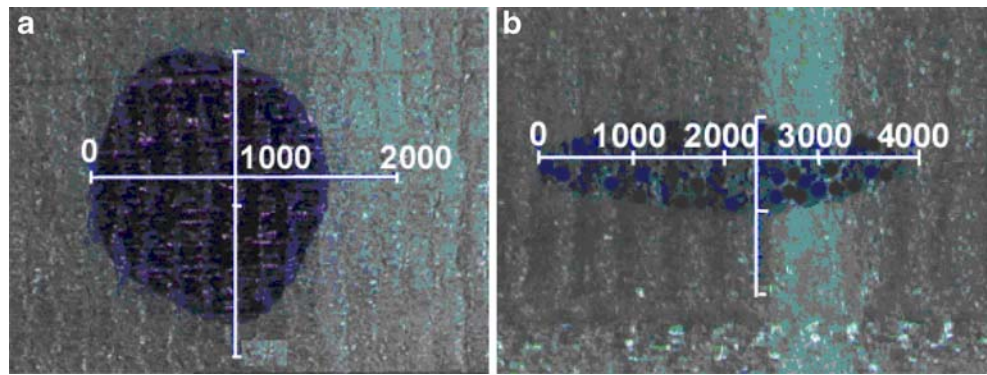
Tensile tests have been performed on a hydraulic tensile machine MTS Elastomer Test System 831 under regulated temperature in an oven. It was not possible to measure the strain evolution during the test. To obtain the local true strain, specimens were tagged. A painted spot with diameter between 1 and 2 mm was plotted on the middle of the specimen. The comparison of the two pictures of the spot, before and after the tests (Fig. 2) enables the determination of the local strain undergone by the material.

Once the specimen was set up in the oven of the tensile machine, it was heated during 8 min with a set point of 90°C. At the end of the heating time, the tension test is performed with a constant velocity of the traverse. Three different velocities were tested: 10 mm.s<sup>-1</sup>, 33 mm.s<sup>-1</sup> and 66 mm.s<sup>-1</sup>. The initial length of the specimen is 30 mm, corresponding strain rate are then: 0.33 s<sup>-1</sup>, 1.1 s<sup>-1</sup> and 2.2 s<sup>-1</sup> which are significantly lower than strain rates involved in the ISBM process. We proceed that way because higher strain rates generate a viscous dissipation that leads to an important increase of the temperature of the specimen during the test and makes it difficult to manage the model identification. Previous works from Chevalier and Marco [27] showed that the behaviour during a biaxial tension can be represented by a model identified from uniaxial results as far as the equivalent strain is chosen as the Max of the principal strain.

For each velocity, several tests were interrupted at different elongation levels. As soon as the test was interrupted, the strain was maintained and the specimen was cooled by a jet of liquid nitrogen to freeze the microstructure. The local evolution of the microstructure was characterised by a differential density measurement in water and air, which was directly linked to crystallinity. Even if the variation of density could not be fully attributed to crystallinity but to the appearance of a crystalline mesophase, the evolution of density is a relevant microscopic parameter depicting the evolution of molecular microstructure. Nevertheless, this microstructure characterisation is not able to take into account its potential anisotropy.

The uniaxial Cauchy stress and the crystallinity versus the longitudinal logarithmic strain are plotted on Fig. 3. Several tests are performed and repeated at different speed conditions for one temperature: a good repeatability can be noted in Fig. 3. The strain-stress curves shapes are similar to previous results obtained by Chevalier and Marco [27] with less dispersion, although heating procedure is different. Stress evolutions for tests at 33 mm.s<sup>-1</sup> and 66 mm.s<sup>-1</sup> are very close, but a significant gap exists with 10 mm.s<sup>-1</sup> tests.

**Fig. 2** Tag of a specimen **a** before and **b** after the tensile test



The interruption at different elongations enables the determination of the crystallinity evolution during the tension tests. It appears that the crystallinity depends more on the uniaxial elongation than on the velocity for the given condition ranges. That is in agreement with the proposed model of induced crystallinity presented by Doufas et al. [32]. Crystallinity presents a notable scattering from one

test to another, as it has also been observed by Ahzi [33]. One may quantify the effect of this scattering by using a stochastic approach, but it seems that it has no significant effect on the mechanical behaviour. We believe that the scattering could be due to the cooling process which is not perfectly reproducible. In the following, mean data are used for identification.

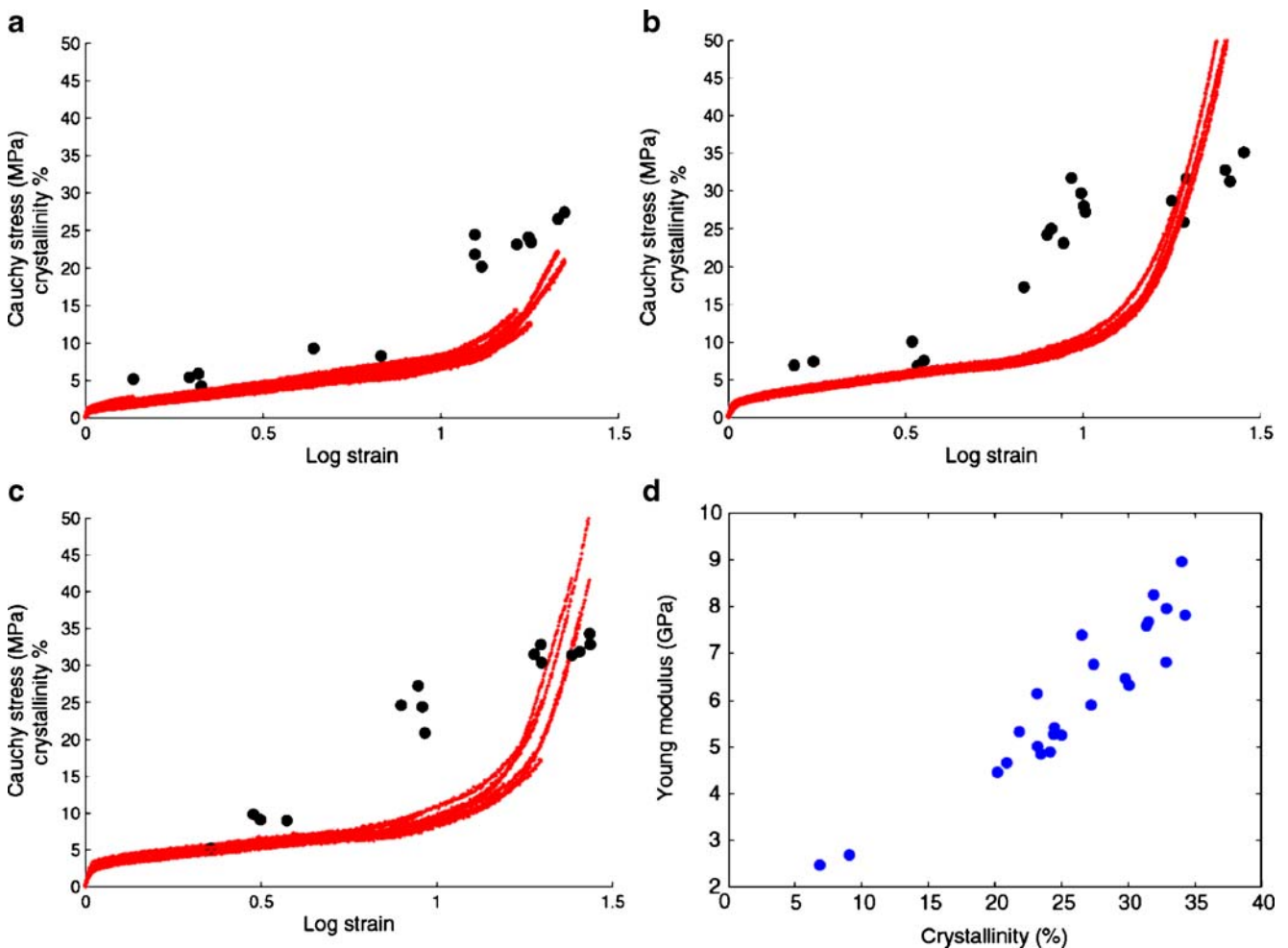


**Fig. 3** Uniaxial tension tests results: lines are uniaxial stress (MPa) and marks are crystallinity ratio (%) for three traverse speeds: **a**  $V=10 \text{ mm.s}^{-1}$ , **b**  $V=33 \text{ mm.s}^{-1}$ , **c**  $V=66 \text{ mm.s}^{-1}$ , **d** Young's modulus versus crystallinity



### Elastic moduli measurements

The measurements were done at room temperature thanks to a mechanical extensometer according to the standard ISO 527. Figure 3d shows the Young modulus of the previously stretched specimen. A relatively good correlation between induced crystallinity and Young modulus is found. This variation of Young modulus is very important (from 2 to 9 GPa) and has an important effect on the rigidity of the blown bottle.

### Measurements on blown bottles

Additional measurements have been performed to provide data to identify the material constitutive law during stretching and to validate the chosen behaviour laws by comparing simulations with experiments on more realistic cases.

### Free blowing of preforms

PET preforms with an initial uniform temperature have been blown without mould (free-blowing) with an internal pressure up to 0.6 MPa. Preforms were first heated in a convection oven to obtain a homogeneous temperature of 96°C during 10 min. Tests had only been performed at 96°C to make sure that non thermal crystallization occurred during the heating step and that the PET was “fluid” enough to make blowing possible considering the decrease of temperature during the transfer between the oven and the blowing apparatus.

Then preforms were quickly transferred in the blowing machine (Fig. 4) and the evolution of the shape of the blown preform was followed using a CCD camera. The results were used in the identification process of the anisotropic constitu-



Fig. 4 Free-blowing test machine of preforms

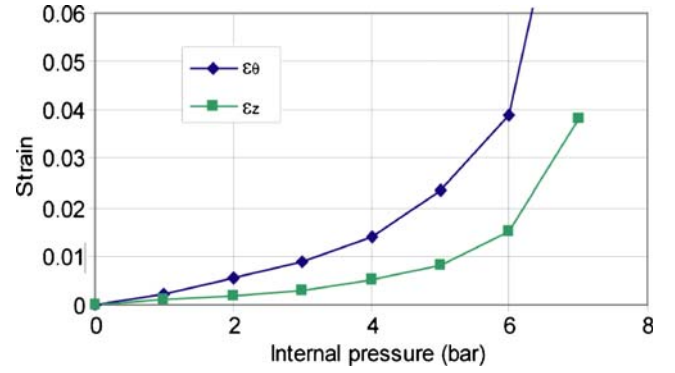


Fig. 5 Circumferential and longitudinal strains measured by the digital images correlation technique

tive law, essentially the final aspect ratio between the length and the diameter of the “bottle”.

### Determination of elastic properties of blown PET bottles

Measurements of Young modulus on PET bottles have been made at room temperature. In a previous article, Chevalier et al. [17] cut out thin specimens in the longitudinal and circumferential directions to measure both longitudinal and circumferential elastic modulus.

Here, moduli have been determined on 2 litres PET soda bottles using a digital correlation technique as deformation measurement. The cylindrical part of the bottle is painted in black and sprayed with white spots. Internal pressure increases from 0 to 7 bars and pictures were taken every bar.

The digital correlation technique allows to determine both circumferential and longitudinal strains  $\epsilon_\theta$  and  $\epsilon_z$  (Fig. 5). The strain dispersion is evaluated to  $3.10^{-4}$ , which is clearly negligible compared to the measured strains. One can see that the mechanical behaviour is nearly linear between 1 and 4 bars but it becomes non linear when a pressure of 5 bar is reached. The yield stress of PET seems to be reached between 6 and 7 bars. The elastic behaviour is considered to be linear until 4 bars.

Longitudinal and circumferential stresses in the cylindrical region of the bottle can easily be estimated from the internal pressure  $P$  respectively to:

$$\sigma_z = \frac{PR}{2e} \quad \sigma_\theta = \frac{PR}{e} \quad (1)$$

For  $2R=92.4$  mm and  $e=0.30$  mm, identification of Young modulus can be achieved from orthotropic Hooke’s elastic law:

$$\epsilon_\theta = \frac{\sigma_\theta - \nu_z \sigma_z}{E_\theta}; \epsilon_z = \frac{\sigma_z - \nu_\theta \sigma_\theta}{E_z} \text{ with : } \frac{\nu_z}{E_\theta} = \frac{\nu_\theta}{E_z} \quad (2)$$

The information obtained by the digital image correlation only gives 3 relations (Eq. 2) for 4 unknown characteristics

$E_z$ ,  $E_\theta$  and  $\nu_z$ ,  $\nu_\theta$ ; an assumption is made to solve the system. It is well known that the Poisson ratio of polymers is related to the elastic modulus in the opposite way:  $\nu$  is getting as near of 0.5 as  $E$  is small. Elastomers for example are quasi incompressible and for more rigid polymers ( $E$  increases) the  $\nu$  value is lower. It is also well known that PET moduli  $E_z$  and  $E_\theta$  increase during the injection stretch-blow moulding process, consequently the related Poisson ratio  $\nu_z$  and  $\nu_\theta$  must decrease. The assumption is to chose 0.38 for the higher Poisson ratio. Then, solving Eqs. 1 and 2 with the measured strains (Fig. 5) and the assumption on the Poisson ratio leads to:  $E_\theta=4500$  MPa;  $E_z=3200$  MPa. The two elastic moduli are clearly different which confirms the induced anisotropy. During blowing the increase of modulus is lower than in uniaxial tension, which can be explained by a lower level of molecular orientation.

### Material behaviour modelling

In this section, two constitutive laws are presented: a viscoplastic model coupled to microstructure evolution to simulate the blow-moulding process and a micromechanics-based model to predict the elastic behaviour after the process.

Viscoplastic behaviour of PET coupled to microstructure evolution

The viscoplastic model initially proposed in Chevalier and Marco [27] and extended in Cosson et al. [29] to take into account the induced anisotropy macroscopically, is adapted here to take into account the microstructure (orientation and crystallinity) evolution and its influence on mechanical parameters. From the interrupted tests, we determined an explicit dependence between the strain hardening and the microstructure variables.

#### Induced crystallinity evolution in stretched PET

To model the evolution of the crystallinity, we chose the same modelling as the one presented by Doufas et al. [32]. The measured crystallinity (Fig. 3) can be easily predicted from Eq. 4. This evolution law of the reduced crystallinity  $y$  is derived from Avrami and the influence of the strain is taken into account *via* the equivalent strain rate  $\dot{\varepsilon}_{eq}$ .

$$X_c = X_c^\infty y \quad (3)$$

$$\frac{dy}{dt} = A(T) \dot{\varepsilon}_{eq} (-\ln(1-y+y_0))^{\frac{m-1}{n}} (1-y) \quad (4)$$

$$\dot{\varepsilon}_{eq} = \max_{i=1,2,3} (\dot{\varepsilon}_i) \quad (5)$$

$\dot{\varepsilon}_i$  are the eigenvalues of the strain rate tensor  $\underline{\underline{D}}$ . Equation 4 is enriched by the initial crystallinity  $y_0$ . In the case of the stretch blow moulding process of PET bottles,  $y_0$  comes from a thermal crystallisation due to the injection of the preform.  $X_c^\infty$  is the ultimate crystallinity.  $A(T)$  is a function dependant on the temperature (Fig. 6a). The Avrami's exponent  $n$  is dependant on the orientation of macromolecules and varies from 1 for uniaxial growth of crystalline lamellas, to 3 for spherulites in quiescent crystallization. We have assumed that an average value  $n=2$  allows an accurate simulation in cases of biaxial tension occurring during stretch blow moulding.

#### Anisotropic viscoplastic behaviour of PET

The viscoplastic model used for the stretch blow moulding process simulation is based on the anisotropic power law viscous model presented in Cosson et al. [29] which includes the strain hardening effect via the consistency  $K$  function of the strain state. The incompressibility condition is still assumed and gives  $\text{tr}(\underline{\underline{D}}) = 0$ . In the new behaviour law, the evolution of  $K$  related to crystallization is by Eqs. 5, 6, 7, 8, 9, and 10 while the evolution of crystallinity is given by Eq. 4. Viscosity is represented by a fourth order tensor:

$$\underline{\underline{\sigma}} = 2\underline{\underline{\eta}} \underline{\underline{D}} - p\underline{\underline{1}} \quad (6)$$

$$\eta_{ijkl} = \eta_{jikl} = \eta_{ijlk} = \eta_{jilk} = \eta_{klij} \quad (7)$$

where  $\underline{\underline{\sigma}}$  is the Cauchy stress tensor.  $\underline{\underline{\eta}}$  is symmetric and is described in the basis of eigenvectors of the tensor  $\underline{\underline{\varepsilon}}$ . All its components are equal to zero except the diagonal terms. Components of the viscosity tensor are strain rate dependant *via* a power law:

$$\eta_{ijkl} = \begin{cases} K_i \bar{\gamma}^{m-1} \delta_{ik} \delta_{jl} & \text{if: } i = j \\ K_\alpha \bar{\gamma}^{m-1} \delta_{ik} \delta_{jl} & \text{if: } i \neq j \text{ with: } \alpha \neq i \neq j \end{cases} \quad (8)$$

$$\bar{\gamma} = \sqrt{2\text{tr}(\underline{\underline{D}}^2)} \quad (9)$$

$$K_i = K_0(T) \exp(\beta_v(\varepsilon_i - \underline{\underline{\varepsilon}})) \times \exp\left(a\left(\frac{1-y_0}{1-y}\right) + b\left(\frac{y-y_0}{1-y_0}\right)^p + c\left(\frac{y-y_0}{1-y_0}\right)\right) i = 1, 2, 3 \quad (10)$$

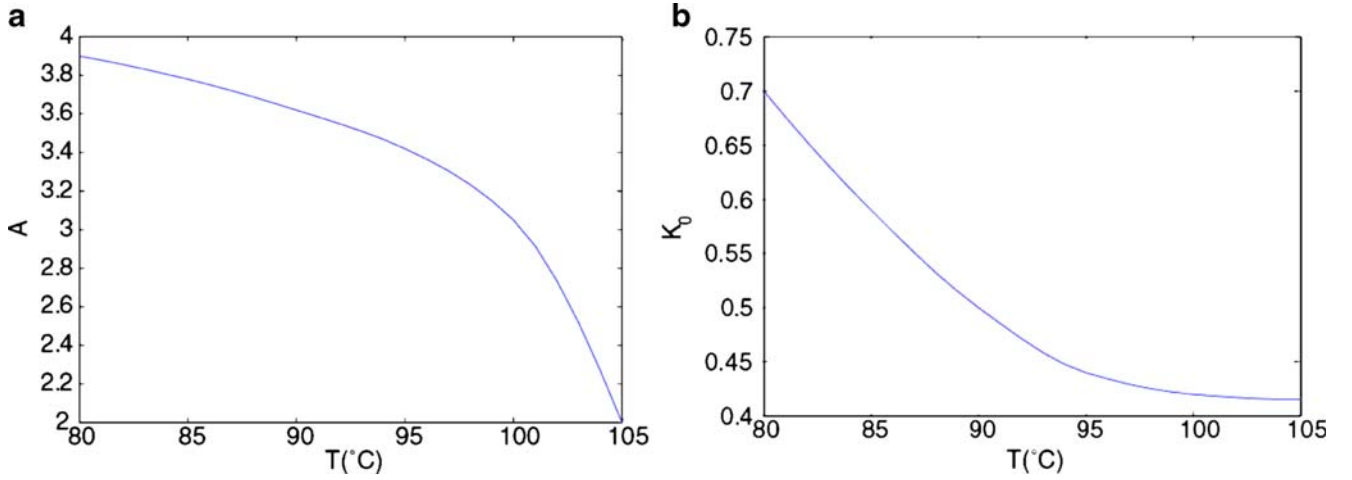


Fig. 6 Factor  $A(T)$  and Factor  $K_0(T)$  in  $\text{MPa}\cdot\text{s}^m$  versus temperature

The effect of structural hardening is given by  $K_i$ . This variable varies exponentially with the crystallinity  $y$ ,  $K_0(T)$  is a factor which depends on the temperature (Fig. 6b).  $\varepsilon_i$  ( $i=1,2,3$ ) are the eigenvalues of the Eulerian logarithmic strain tensor ( $\underline{\underline{\varepsilon}} = \frac{1}{2} \log(\underline{\underline{B}})$  where  $\underline{\underline{B}}$  is the left Cauchy-Green tensor) and  $\underline{\underline{\varepsilon}}$  is the maximum value of  $\varepsilon_i$  on  $i=1,2$  or 3.  $\beta_v$  is a factor of anisotropy; a zero value for  $\beta_v$  is representative of an isotropic behaviour. The numerical values of the parameters of the model, identified from the tension tests presented in the previous section, are given in Table 1.

#### Determination of the crystalline-dependant elastic behaviour

During the stretch blow moulding process of PET bottles, the microstructure of the material is changing from a nearly isotropic amorphous state to a strongly anisotropic semi-crystalline state with a concentration of crystals that can reach nearly 40%. In the case of stretch blow moulding process, one or two directions are highly stretched, while the third direction undergoes a contraction, the final material is considered as orthotropic.

The value of the mechanical property in the thickness direction has a very small influence on the global behaviour of the bottle. Finally, we have assumed a transverse isotropic behaviour with identical properties in second and third direction.

The semicrystalline PET was modelled as a composite matrix-inclusion, where the matrix represents the amorphous phase and inclusions represent crystals. Rutledge [34] shows that PET crystals have isotropic transverse

elastic properties and geometry. They can be modelled like spherical inclusions as in Bedoui et al. [35].

$$C_{crystal} = \begin{bmatrix} 118000 & 5700 & 5700 & 0 & 0 & 0 \\ 5700 & 7700 & 5460 & 0 & 0 & 0 \\ 5700 & 5460 & 7700 & 0 & 0 & 0 \\ 0 & 0 & 0 & 2240 & 0 & 0 \\ 0 & 0 & 0 & 0 & 3240 & 0 \\ 0 & 0 & 0 & 0 & 0 & 3240 \end{bmatrix} \text{ (MPa)} \quad (11)$$

Micromechanical calculations are based on a model proposed by Walpole [36] and modified by Federico et al. [37]. Both models are derived from Eshelby's problem, which gives the solutions for fields of stress and strain of an ellipsoidal inclusion surrounded by an isotropic infinite matrix. The exact solution is known for a spheroid inclusion with an isotropic transverse behaviour, of which the isotropic transverse axis is confused with the axis of symmetry of the inclusion. The strain in the inclusion depends on the strain imposed towards infinity (Eq. 12).

$$\underline{\underline{\varepsilon}} = \underline{\underline{A}} \underline{\underline{\varepsilon}}^\infty \quad (12)$$

$$\underline{\underline{A}} = \left[ \underline{\underline{I}} + \underline{\underline{S}} : \left( \underline{\underline{C}}_0^{-1} : \underline{\underline{C}}_i - \underline{\underline{I}} \right) \right]^{-1} \quad (13)$$

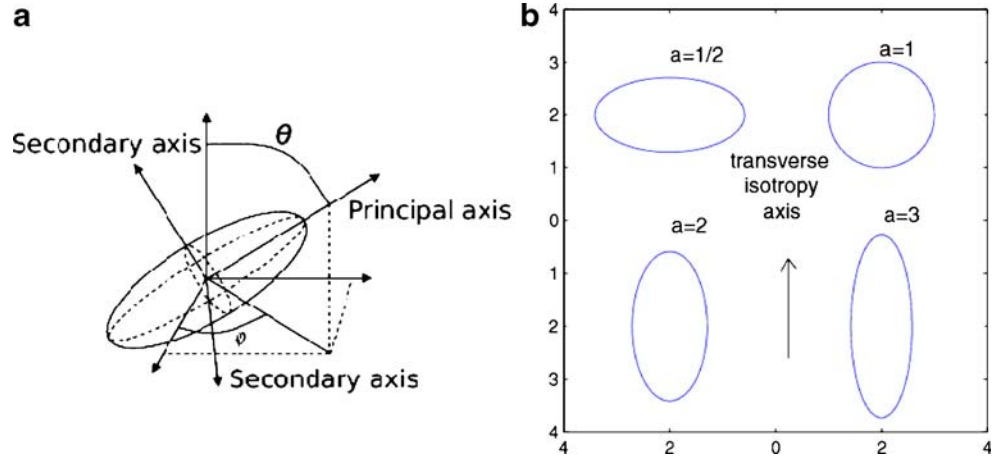
$\underline{\underline{A}}$  is the strain localization tensor,  $\underline{\underline{C}}_0$  and  $\underline{\underline{C}}_i$  are respectively the elastic tensors of matrix and inclusion,  $\underline{\underline{I}}$  is the identity tensor in the space of fourth order

Table 1 Parameter values of the viscoplastic constitutive law of PET at process temperature

Parameters	$a$	$b$	$c$	$M$	$n$	$p$	$X_c^\infty$	$y_0$	$\beta_v$
Values	0.14	1.85	0.57	0.6	2	0.2	0.36	0.14	3



**Fig. 7** **a** Elliptical inclusion location defined by angles  $\theta$  and  $\phi$ , **b** Various inclusion shape factors



symmetrical tensor and  $\underline{\underline{S}}$  is the Eshelby's tensor which depends only on the Poisson's coefficient of the matrix and shape factor of inclusion (Fig. 7).

$$\underline{\underline{C}} = \left[ \sum_{r=0}^N c_r \underline{\underline{C}}_r : \underline{\underline{A}}_r \right] : \left[ \sum_{r=0}^N c_r \underline{\underline{A}}_r \right]^{-1} \quad (14)$$

$$\sum_{r=0}^N c_r = 1 \quad (15)$$

Equation 14 gives an estimation of the elastic tensor of the effective media for a mixture of  $N+1$  phases (phase 0 is the matrix). For the matrix, the Eshelby's tensor is identity. Each one of  $N$  phases is composed of identical inclusions: they have the same orientation, shape factor and elastic properties.  $c_r$  gives the volume fraction of each phase. In the case of bi-stretched PET we have a statistical distribution of crystals. This distribution is considered as transverse isotropic to be consistent with the previous assumption made on the viscoplastic behaviour. Two angles ( $\theta$  and  $\varphi$ ), are needed to define the orientation of inclusion as illustrated in Fig. 7. If we consider the average distribution, a unique isotropic transverse inclusion remains. Equation 14 can be rewritten as follows:

$$\underline{\underline{C}} = \left[ (1-c) \underline{\underline{C}}_0 + c \int_{\mathbb{S}^{2+}} \psi \underline{\underline{C}}_i : \underline{\underline{A}}_i da \right] : \left[ (1-c) \underline{\underline{I}} + c \int_{\mathbb{S}^{2+}} \psi \underline{\underline{A}}_i da \right]^{-1} \quad (16)$$

$$\int_{\mathbb{S}^{2+}} \psi da = 1 \quad (17)$$

$\mathbb{S}^{2+}$  is the half unit sphere, which describes all directions in space in 3 dimensions.  $\psi$  is the probability density of the orientation of inclusion and  $c$  is the volume fraction of crystals.

#### Distribution density of inclusion orientation

The transverse isotropy requires  $\psi$  to be independent of the variable  $\varphi$  (i.e.  $\psi(\theta, \varphi) = \psi(\theta)$ ). We propose a density of distribution which is a function of the strain tensor's principal values (Fig. 8). If the material is not stretched, the deformation is isotropic and the density of distribution does not depend on the orientation ( $\psi(\theta) = \pi/2$ ).

$$g(\theta) = \left( (1 - \chi^2) \left( 1 + \exp \left( \frac{\theta - \frac{\pi}{2} \chi^{1/2}}{\chi^2} \right) \right) \right)^{-1} + \chi^2 \quad (18)$$

$$\psi(\theta) = \frac{g(\theta)}{2\pi \int_0^{\pi/2} g(\theta') \sin(\theta') d\theta'} \quad (19)$$

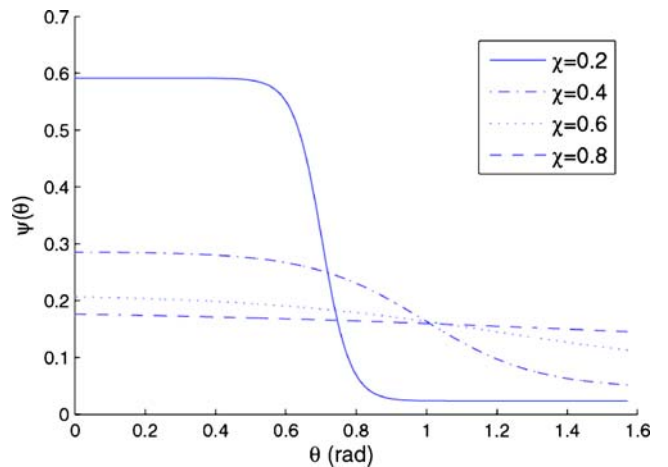


**Fig. 8** Density distribution of inclusion orientation  $\psi(\theta)$  for various values of strain level  $\chi$

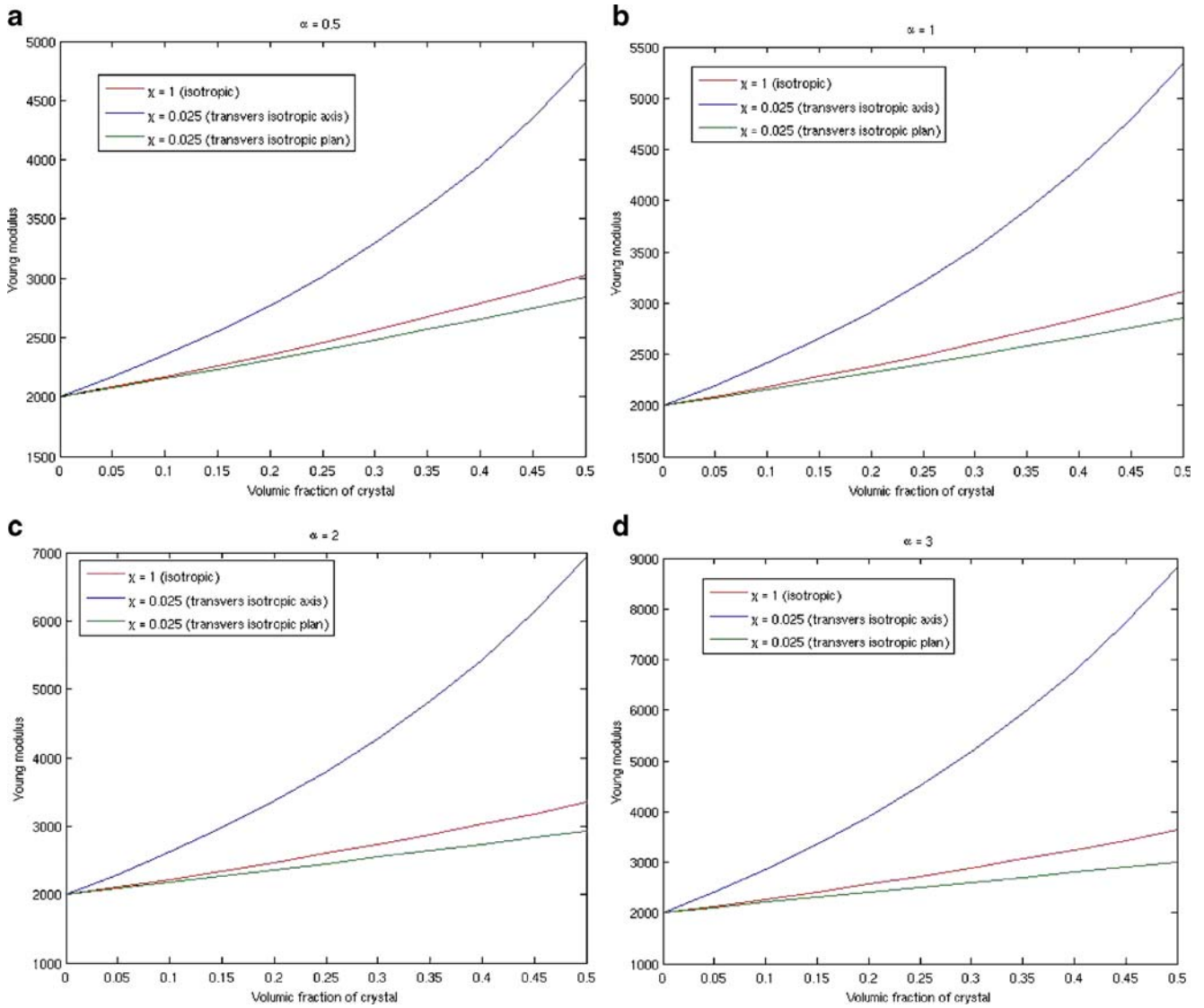


Fig. 9 Estimation of Young's modulus for various values of inclusion shape factor

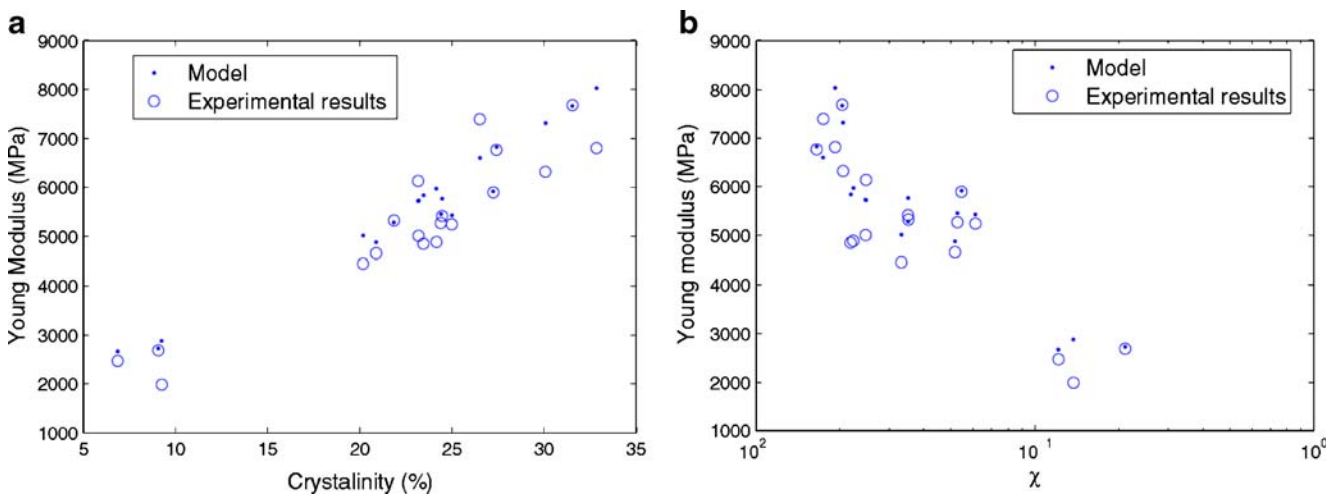


Fig. 10 Young modulus versus a crystallinity and b strain level

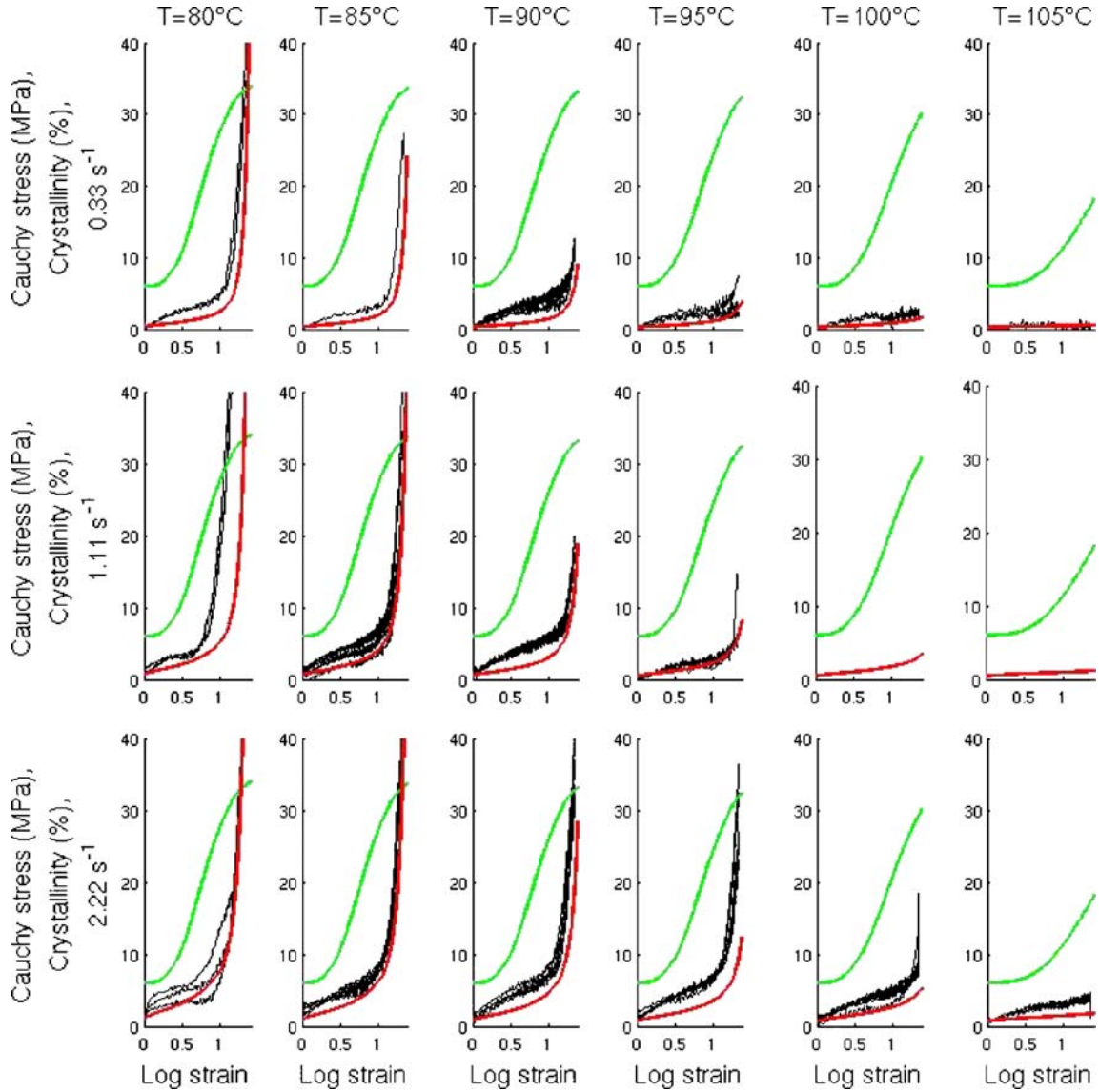


Fig. 11 1D simulations of tension tests, lower curve is stress in MPa, upper curve is crystallinity ratio

$$\chi = \exp(\beta_e(\varepsilon_{II} - \varepsilon_{III})) \quad \text{with: } \varepsilon_I \varepsilon_{II} \varepsilon_{III} \quad (20)$$

where the  $\varepsilon_k$  ( $k=I, II, III$ ) are the principal values of the strain tensor and  $\chi$  is a function that represents the strain level:  $\chi=1$  means that the material is not stretched and is isotropic,  $\chi=0$  means that all crystals are oriented in the same direction.

#### Influence of inclusion shape factor

Figure 9 shows the influence of inclusion shape factor on effective modulus of homogenized media. The higher the shape factor, the more the properties following the plan of transverse isotropy and transverse isotropy axis are different.

For the modulus measurements given on Fig. 3(d), the shape factor was identified to  $\alpha=5$  for the coefficient  $\beta_e=2$ .

The predictions of the model given by Eq. 17 are compared with experimental values in Fig. 10(a) according to the measured crystallinity in Fig. 10(b) and the elongation represented by  $\chi$ . One can see that experimental data and model simulation superpose well on both graphs. The modelling of this step is accurate. As given in Goschel [38] the Young modulus of the amorphous phase is equal to 2 GPa in this calculation.

#### Simulations

Numerical simulations of the stretch blow moulding process have been done using the meshless method called C-NEM. The aim of this paper is not to make theoretical developments on C-NEM and interested readers will find

details in Yvonnet et al. [39] for example. Nevertheless, this method is well adapted to simulations involving large distortions of the initial “mesh”. For sake of simplicity, elastic simulations of the behaviour of bottles under internal pressure have also been made with C-NEM. In that case, strains remains small and the benefit of the C-NEM method is poor, a finite element mesh based on the Delaunay triangulation of the node distribution would give as accurate results as C-NEM method with a lower cost.

Identification and validation of the modelling  
by simulations

#### *Simulation of the uniaxial tension tests*

Figure 11 shows the numerical simulations of the tensile tests that have been made to validate the identified constitutive laws. The evolution of the stresses closely reproduces the experimental results published by Chevalier et al. [27] for different initial strain rates ( $0.33 \text{ s}^{-1}$ ,  $1.11 \text{ s}^{-1}$  and  $2.22 \text{ s}^{-1}$ ) and temperatures (from  $80^\circ\text{C}$  to  $100^\circ\text{C}$ ).

The proposed simulation allows the determination of the microstructure state (direction and crystallinity) at any moment, especially at the end of the blowing. This description of the microstructure will enable us to predict the elastic behaviour of the bottle at room temperature thanks to a micromechanics post processing.

#### *Identification of anisotropic parameter $\beta_v$ by simulation of the free blowing tests*

To identify the optimum value of the coefficient  $\beta_v$  an inverse technique was performed from several free blowing experiments of PET preforms (Fig. 4). The initial temperature was uniform ( $96^\circ\text{C}$ ) and the internal pressure equal to 0.6 MPa. The average of final heights ( $H_{real}$ ) and the average of final diameters ( $d_{real}$ ) were respectively 33.8 cm and 10.6 cm (Fig. 12). Numerical simulations of free blowing were run for different values of  $\beta_v$ . We compared the two lengths of bottles with the simulated ones. The optimum value of the coefficient  $\beta_v$  is 3. It is the value that minimizes the following expression:

$$\Phi(\beta) = \frac{\sqrt{(d_{real} - d_{sim}(\beta))^2 + (H_{real} - H_{sim}(\beta))^2}}{\sqrt{d_{real}^2 + H_{real}^2}} \quad (21)$$

where  $H_{sim}$  and  $d_{sim}$  are, respectively, the height and the diameter of simulated bottles. This value is obtained for the simulation shown in Fig. 12. For  $\beta_v < 3$  bottles are too short and for  $\beta_v > 3$  bottles are too long. In all simulations the value of the diameter is about 10.5 cm.  $\beta_v$  only affects the length of the bottle.

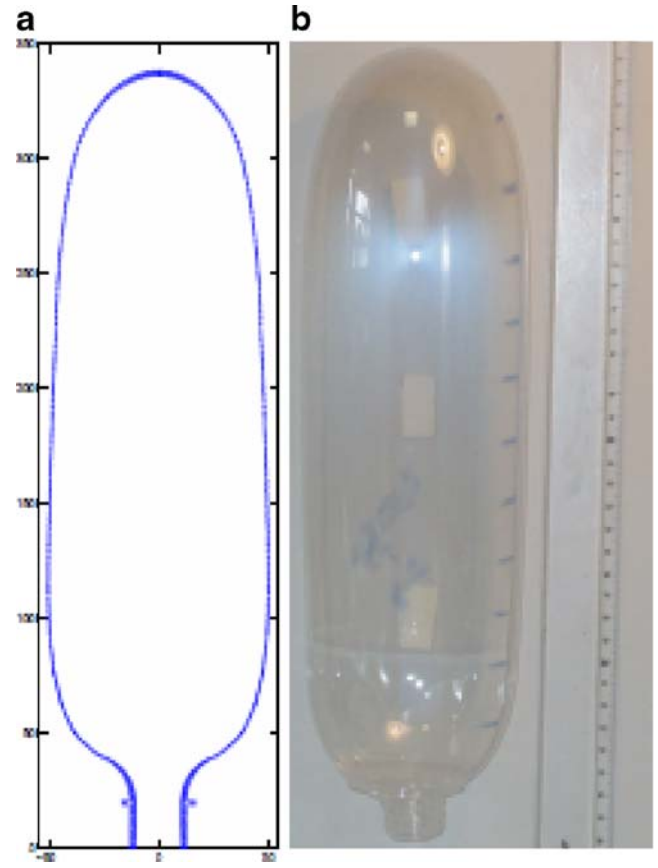


**Fig. 12** Comparison between measurement and simulation for a free blowing with an internal pressure  $P_i=0.6 \text{ MPa}$  and a homogeneous temperature  $T_0=96^\circ\text{C}$  **a** simulation of free blowing with  $\beta_v=3$ , **b** free blowing bottle

Simulation of the stretch blow moulding process for 2 L and 0.33 L bottles

We simulated the stretch blow moulding process for two performs of 2 L and 0.33 L bottles, respectively 40 g and 25 g. Stretch blow-moulding simulations have been managed using the following conditions: rod speed= $1 \text{ m}\cdot\text{s}^{-1}$ , initial temperature  $103^\circ\text{C}$  and blowing pressure 7 bar for the 2 L bottle; rod speed= $1.2 \text{ m}\cdot\text{s}^{-1}$ , initial temperature  $101^\circ\text{C}$  and blowing pressure 7 bar for the 0.33 L bottle. Figure 13 represents the evolution of the perform’s shapes for both cases. These simulations were performed on a desktop PC (Pentium 4 3.4 GHz) in less than 2 h, without remeshing and adding nodes.

The influence of processing parameters (initial temperature profile in the perform, speed of the elongation rod, delay between elongation and blowing...) will be studied later in another paper in order to determine their effect and optimize the elastic properties as presented in Cosson et al. [29] for a less advanced model.

Here, the viscoplastic model, coupled to the microstructure, allows the determination of the microstructural



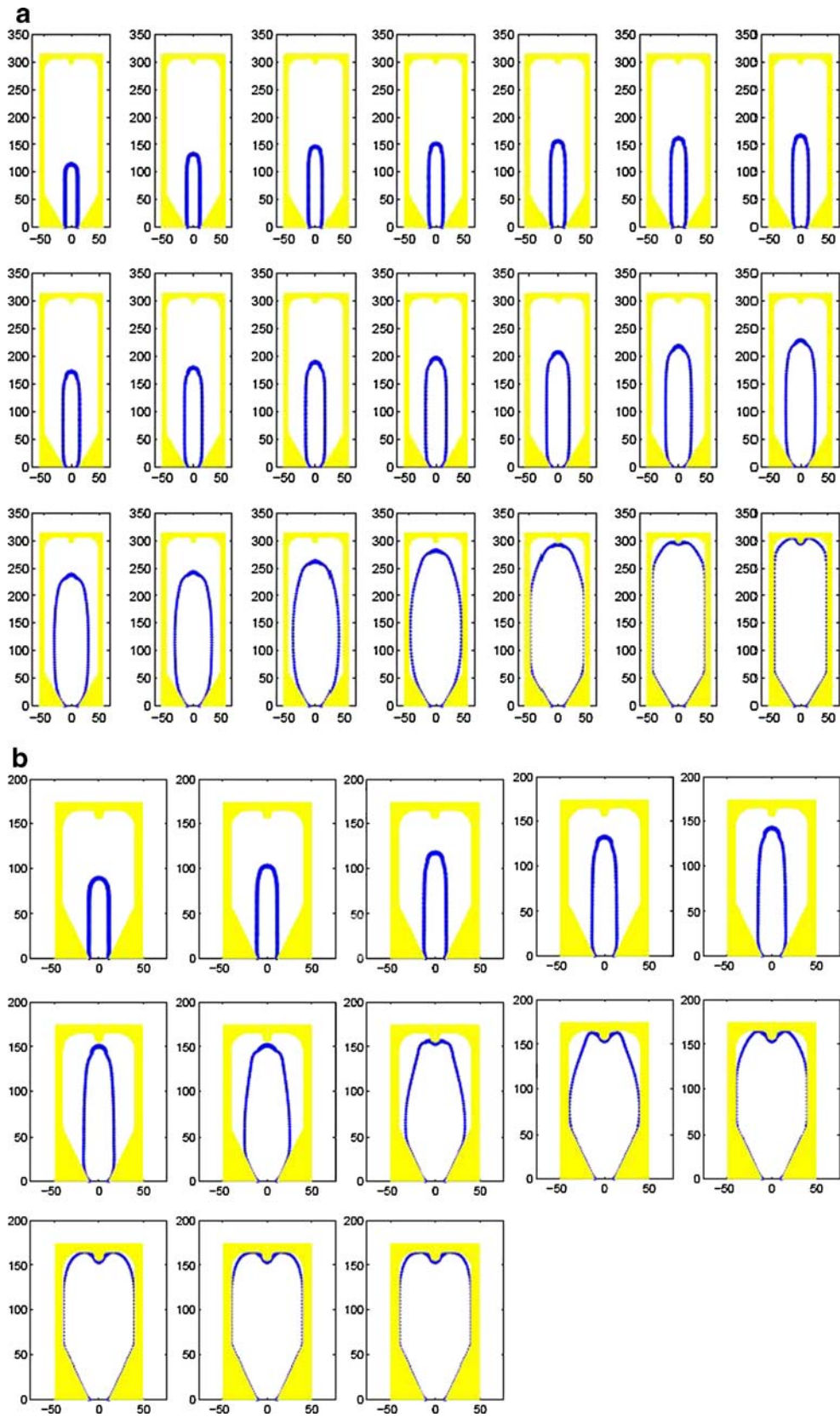


Fig. 13 Simulated evolution of preform in a 2 L mould and b 0.33 L mould



variables evolution versus time during the process. Especially, when the final shape of the bottle is obtained, these variables are used for micromechanical calculations to predict the elastic properties of bottles at room temperature. Figure 14 shows the crystallinity distribution in bottles of 0.33 L and 2 L. The bottoms of the bottles are thick: this is due to the stretch rod in contact with the material that leads to a zone where PET is not stretched. As a consequence, the rigidity does not increase in the bottom of the bottles and the crystallinity remains low. Figure 14 represents also the Young modulus in the first and second principal strain directions at each node of the final bottle.

Application: the design of bottles

The numerical simulation is often used to evaluate the strength of a newly designed PET bottle. From the CAD file used for the geometrical definition of the bottle and the mould one can easily provide a finite element mesh and run an elastic simulation of a top load test, a creep under pressure, or a burst test... The mechanical properties needed as input of this elastic calculation at room temperature are obtained from the anisotropic homogenization calculation.

Here, the input data is obtained from the viscoplastic simulation (Fig. 13) *via* the micromechanical calculation presented in “Determination of the crystalline-dependant elastic behaviour”. The anisotropic behaviour law (Eq. 16) is used.

These results ( $E_{\theta}=5$  GPa,  $E_z=4$  GPa in the cylindrical region of the bottle) may be compared with measurements done on soda bottles and presented in section “Experimental”. Considering the complexity of the process and the various steps involved in the simulation, the comparison, which highlights about 15–20% difference, is satisfactory. This difference could be explained by many reasons: mode of deformation, strain rate, cooling rate, contact conditions,

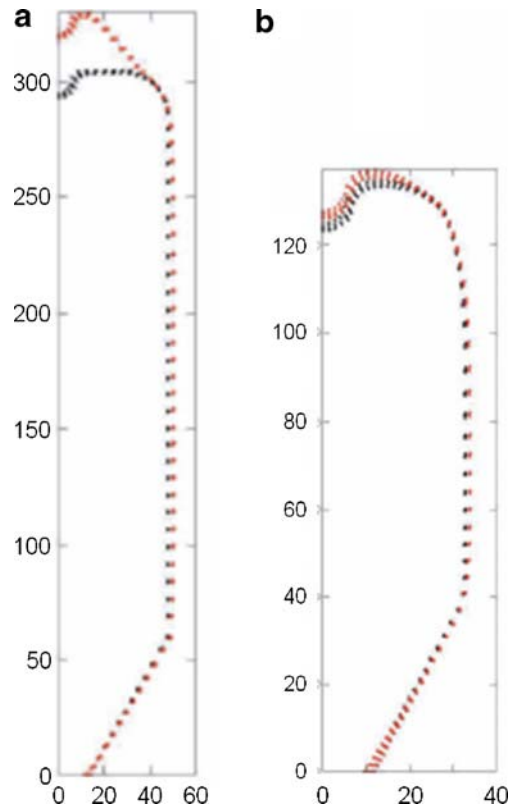


Fig. 15 Deformed bottles under internal pressure for **a** the 2 L bottle and **b** the 0.33 L bottle. All dimensions are in mm

injection conditions of the preform for example. A better description of the initial temperature conditions of the stretch blow moulding process and the use of a more realistic blowing pressure evolution, as presented in Menary et al. [40] or Cosson et al. [41], for example, would also improve the predictions.

We have also studied the deformation of bottles under pressure. As PET is widely used for storing soft drinks, the

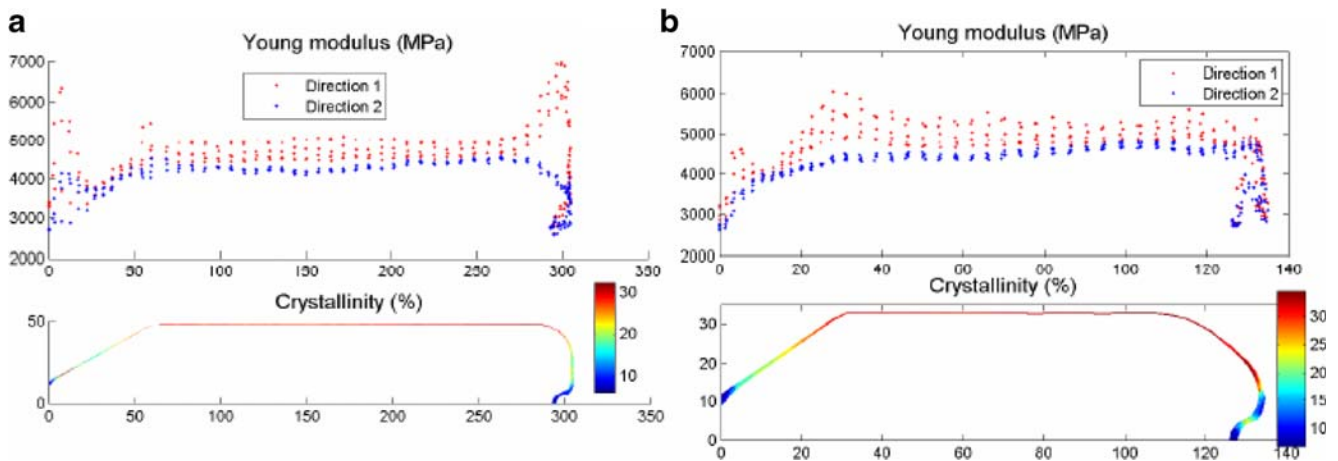


Fig. 14 Prediction of crystallinity and corresponding Young modulus **a** 2 L bottle –40 g preform, **b** 2 L bottle –25 g preform

bottle shape should not significantly change even if the internal pressure varies with ambient condition (temperature). Figure 15 shows the 2 L and 0.33 L deformed bottles under an internal pressure of 4 bars. We can notice that the 0.33 L bottle resists to pressure, the deformed shape does not vary much from the initial shape. For the 2 L bottle, the base is much more deformed; this is due to its flat bottom and it is a consequence of the axisymmetric modelling. In a 3D modelling, the real geometry of the base would certainly lead to a different conclusion.

For anisotropic elastic simulation at room temperature, the C-NEM method is convenient because the position of the nodes at the end of the blow-moulding simulation is directly used to define the geometry of the bottle. Nevertheless, considering the small strain involved in this simulation, it should have been possible to use the finite element method.

## Conclusions

The different steps presented in this work provide a complete analysis of the stretch blow-moulding process, from the simulation of the process to the prediction of the elastic properties of the bottle. We built a simple viscoplastic model that can take into account the evolution of the microstructure and that represents the anisotropic behaviour of PET during the stretch blow-moulding process.

In the simulation, we have computed the evolution of the molecular orientation and the crystallinity at each step of the process. A micromechanic modelling makes use of this final microscopic data to predict the final anisotropic elastic behaviour of the bottle at room temperature.

The developed tools provide useful information for the design of PET bottle. Before manufacturing expensive tools, the optimization of the bottle geometry can be done from simulations. All these predictions of mechanical properties need an accurate knowledge of the material properties that can be provided by the simulation of the blow moulding step.

Further work has to be done in order to extend the simulation to 3D geometry and not only axis-symmetric ones. Another important improvement of our work would be to replace the thermo-dependent viscoplastic model by a viscoelastic one during the blowing. Recent experiments made on petaloid bases of PET bottles by some of the authors should provide a useful database to extend the whole modelling to 3D.

**Acknowledgement** The authors are grateful to Richard Parker for English improvements in the text and Sidel group which let us their free blowing apparatus and provided preforms.

## References

1. Daubeny RP, Bunn CW (1954) The crystal structure of polyethylene terephthalate. *CJ Proc R Soc Lond A* (226):531–542
2. Benatmane A (1992) Etude du vieillissement physique du poly(ethylene terephthalate) amorphe et semi-cristallin, Ph D Thesis, INSA-Lyon
3. Hieber CA (1995) Correlation for the quiescent crystallization kinetics of isotactic polypropylene and poly(ethylene terephthalate). *Polymer* 36(7):1455–1467
4. Asano T, Seto T (1973) Morphological Studies of Cold Drawn Poly(ethylene terephthalate). *Polymer* 5(1):72–85
5. Fisher EW, Fakirov S (1976) Structure and properties of polyethylene terephthalate crystallized by annealing in the highly oriented state. *J Mater Sci* 11:1041
6. Shen D, Fujin L, Zaiqing W, Renyuan Q (1991) Conformational changes of amorphous PET films during uni-axial stretching. *Makromol Chem*, 301–307
7. Spiby S, O'Neil MA, Duckett RA, Ward IM (1992) An infra-red study of conformational changes occurring during the drawing of PEMT, PET and PEMT/PET copolymers. *Polymer* 33:4479–4485
8. Lapersonne P, Bower DI, Ward IM (1992) Molecular orientation and conformational changes due to uniaxial-planar deformation of PET. *Polymer* 33:1277–1283
9. Pople JA, Mitchell GR, Sutton SJ, Vaughan AS, Chai CK (2000) The development of organized structures in polyethylene crystallized from a sheared melt, analyzed by WAXS and TEM. *Polymer* 40:2769–2777
10. Titomanlio G, Speranza V, Brucato V (1997) On the simulation of thermoplastic injection moulding process. *Intern Polym Processing* 12:45–53
11. Salem DR (1992) Development of crystalline order during hot drawing of poly(ethylene terephthalate) film: influence of strain rate. *Polymer* 33(15):1382–1388
12. Marco Y, Chevalier L, Chaouche M (2002) WAXD study of induced crystallization and orientation in poly(ethylene terephthalate) during biaxial elongation. *Polymer* 43:6569–6574
13. Le Bourvellec G, Beautemps J (1990) Stretching of PET films under constant load II structural analysis. *J App Pol Sci* 39:329–339
14. Vigny M, Tassin JF, Gibaud A, Lorentz G (1997) Study of the molecular structure of PET films obtained by an inverse stretching process Part 1: constant speed drawing of amorphous films. *J Polym Eng Sci* 37(11):1785–1794
15. Hanley T, Sutton D, Cookson D, Kosior E, Knott R (2006) Molecular morphology of petaloid bases of PET bottles: a small-angle X-ray scattering study. *J Appl Polym Sci* 99(6):3328–3335
16. Picard M, Billon N (2007) Microstructural evolution of PET under stretching and during stretch blow moulding, 10th Int Esaform Conference on Material Forming, Zaragoza, Spain, 907, 801–806
17. Chevalier L, Linhone C, Regnier G (1999) Induced crystallinity during stretch-blow moulding process and its influence on mechanical strength of poly(ethylene terephthalate) bottles. *Plast Rubber Compos* 28(8):393–401
18. Mir H, Benrabah Z, Thibault F (2007) The use of elasto-visco-plastic material model coupled with pressure-volume thermodynamic relationship to simulate the stretch blow molding of polyethylene terephthalate. *AIP Conference proceedings*, 908, 331–336
19. Pham X-T, Thibault F, Lim L-T (2004) Modeling and simulation of stretch blow moulding of polyethylene terephthalate. *Polymer Eng Sci* 44(8):1460–1472
20. Haddad H, Masood S, Erbulut DU (2009) A study of blow moulding simulation and structural analysis for PET bottles. *Australian J Mech Eng* 7(1):69–76
21. Bagherzadeh S, Biglari FR, Nikbin K (2010) Parameter study of stretch-blow moulding process of polyethylene terephthalate

- bottles using finite element simulation. Proceedings of the Institution of Mechanical Engineers, Part B: J. of Eng. Manufacture 224(8):1217–1227
22. Michaeli W, Leopold T (2010) Modelling the structural performance of stretch-blow moulded PET bottles. Annual technical Conference—ANTEC, Conference Proceedings 1:333–337
  23. Menary G, Armstrong CG, Crawford RJ, McEvoy JP (2000) Modelling of poly(ethylene terephthalate) in injection stretch-blow moulding. *Plast Rubbers Compos* 29(7):360–370
  24. Marckma G, Verron E, Peseux B (2001) Finite element analysis of blow molding and thermoforming using a dynamic explicit procedure. *Polymer Eng Sci* 41(3):426–439
  25. Gorlier E, Agassant J-F, Haudin J-M, Billon N (2001) Experimental and theoretical study of the uniaxial deformation of amorphous PET above the glass transition temperature. *Plast Rubber Compos Process Appl* 30(2):48–55
  26. Schmidt FM, Agassant J-F, Bellet M, Dessouter L (1996) Viscoelastic simulation of PET stretch blow moulding process. *J Non Newton Fluid Mech* 64:19–42
  27. Chevalier L, Marco Y (2006) Identification of a strain induced crystallisation model for PET under uni and bi-axial loading: influence of temperature dispersion. *Int J Mech Mater* 39(6):596–609
  28. Bordival M, Schmidt FM, Le Maoult Y, Velay V (2009) Optimization of preform temperature distribution for the stretch-blow moulding of PET bottles: infrared heating and blowing modelling. *Pol Eng Sci* 49(4):783–793
  29. Cosson B, Chevalier L, Yvonnet J (2009) Optimization of the thickness of PET bottle during stretch-blow molding by using a mesh-free (numerical) method. *Int Polymer Process* 24(3):223–233
  30. Buckley CP, Jones DC (1995) Glass-rubber constitutive model for amorphous polymers near the glass transition. *Polymer* 36:3301–3312
  31. Figiel L, Buckley CP (2009) On the modelling of highly elastic flows of amorphous thermoplastics. *Int J Non-Linear Mech* 44:389–395
  32. Doufas AK, McHugh AJ, Miller C (2000) Simulation of melt spinning including flow-induced crystallization—Part II quantitative comparisons with industrial spinline data. *J Non-Newton Fluid Mech* 92:27–66
  33. Ahzi S, Makradi A, Gregory RV, Edie DD (2003) Modelling of deformation behaviour and strain-induced crystallization in poly(ethylene terephthalate) above the glass transition temperature. *Mec Mat* 35:1139–1148
  34. Rutledge GC (1997) Thermomechanical properties of the crystal phase of poly(ethylene terephthalate) by molecular modeling. *Macromolecules* 30:2785–2791
  35. Bédoui F, Diani J, Régnier G, Seiler W (2006) Micromechanical modeling of isotropic elastic behavior of semi-crystalline polymers. *Acta Materialia* 54(6):1513–1523
  36. Walpole LJ (1981) Elastic behaviour of composite materials: theoretical foundations. *Adv Appl Mech* 21:169–242
  37. Federico S, Grillo A, Herzog W (2004) A transversely isotropic composite with a statistical distribution of spheroidal inclusions: a geometrical approach to overall properties. *J Mech Phys Solids* 52:2309–2327
  38. Göschel U (1996) Thermally stimulated structural changes in highly oriented glassy poly(ethylene terephthalate). *Polymer* 37:4049–4059
  39. Yvonnet J, Ryckelynck D, Lorong P, Chinesta F (2004) A new extension of the natural element method for non-convex and discontinuous problems: the constrained natural element method (C-NEM). *Int J Num Meth Eng* 60:1451–1474
  40. Menary G, Tan CW, Armstrong CG, Salomeia Y, Picard M, Billon N, Harkin-Jones EMA (2010) Validating injection stretch blow moulding simulation via freeblow trials. *Polym Eng Sci* 50:1047–1057
  41. Cosson B, Schmidt F, Le Maoult Y, Bordival M (2010) Infrared heating stage simulation of semi-transparent media (PET) using ray tracing method. *Int J Mater Form*. doi:10.1007/s12289-010-0985-8